Random walk particle tracking simulations of non-Fickian transport in heterogeneous media

G. Srinivasan [a,*], D.M. Tartakovsky [b], M. Dentz [c], H. Viswanathan [d], B. Berkowitz [e], B.A. Robinson [d]

[a] Theoretical Division, Los Alamos National Laboratory, Los Alamos, NM 87545, USA
[b] Department of Mechanical and Aerospace Engineering, University of California, San Diego, 9500 Gilman Drive, Mail Code 0411, La Jolla, CA 92093, USA
[c] Institute of Environmental Assessment and Water Research (IDÆA-CSIC), Barcelona, Spain
[d] Earth and Environmental Sciences Division, Los Alamos National Laboratory, Los Alamos, New Mexico, USA
[e] Department of Environmental Sciences and Energy Research, Weizmann Institute of Science, Rehovot, Israel

ARTICLE INFO

ABSTRACT

Derivations of continuum nonlocal models of non-Fickian (anomalous) transport require assumptions that might limit their applicability. We present a particle-based algorithm, which obviates the need for many of these assumptions by allowing stochastic processes that represent spatial and temporal random increments to be correlated in space and time, be stationary or non-stationary, and to have arbitrary distributions. The approach treats a particle trajectory as a subordinated stochastic process that is described by a set of Langevin equations, which represent a continuous time random walk (CTRW). Convolution-based particle tracking (CBPT) is used to increase the computational efficiency and accuracy of these particle-based simulations. The combined CTRW–CBPT approach enables one to convert any particle tracking legacy code into a simulator capable of handling non-Fickian transport.

1. Introduction

Many physical, biological, and biochemical phenomena (e.g., [1–4]) involve a combination of three passive transport mechanisms: advection, molecular diffusion, and hydrodynamic dispersion. Standard mathematical descriptions of such phenomena rely on an advection–dispersion equation (ADE),

$$\frac{\partial c}{\partial t} = \nabla \cdot (\mathbf{D} \nabla c) - \nabla \cdot (\mathbf{v} c), \tag{1}$$

where c is the volumetric concentration of a substance (e.g., solute), $\mathbf{v}$ is the (macroscopic) advection velocity, and $\mathbf{D} = D_m \mathbf{I} + \mathbf{D}_d$ is the dispersion coefficient tensor defined as the sum of the molecular diffusion coefficient D_m ($\mathbf{I}$ being the unit tensor) and the dispersivity tensor $\mathbf{D}_d = \mathbf{D}_d(\mathbf{v})$. Although the ADE proved to be indispensable in describing many transport processes, it has a number of drawbacks and limitations that are both computational and conceptual in nature.

Numerical solutions of the ADE (1) introduce "numerical dispersion", which manifests itself in excessive smearing of concentration profiles at large Péclet numbers. This problem is exacerbated by high degrees of anisotropy that often characterize hydrodynamic dispersion. For example, transport in natural porous media typically exhibit longitudinal dispersivities that are two orders of magnitude higher than their transverse counterparts [5]. Numerical dispersion can be controlled by employing Eulerian–Lagrangian [6,7] and other [8] algorithms, many of which are computationally expensive.

* Corresponding author.
E-mail addresses: gowri@lanl.gov (G. Srinivasan), dmt@ucsd.edu (D.M. Tartakovsky), marco.dentz@idaea.csic.es (M. Dentz).

A more fundamental shortcoming of the macroscale ADE (1) is its inability to capture anomalous or non-Fickian transport behavior, which is often observed in heterogeneous environments [9–14]. This failure can be attributed to subgrid scale heterogeneity that is not resolved at the support scale on which the parameters of the ADE are defined. If it is possible to resolve the heterogeneity structure on all scales, the corresponding ADE reflects the related anomalous transport behavior (e.g., [15]). This is not very realistic for many practical applications.

This shortcoming of the macroscale ADE can be effectively overcome by replacing the ADE (1) with its counterparts that are *nonlocal* in space and/or time. Derivations of nonlocal transport equations rely on a number of assumptions. For example, stochastic derivations of nonlocal mean transport equations often require velocity fluctuations to be either small [16] or Gaussian [17]; and standard derivations of both fractional ADEs (fADEs) [18,19] and effective equations of continuous time random walk (CTRW) models [20–24] are based on the assumption that subgrid scale fluctuations are space–time stationary. Particle-based simulations provide a computationally efficient framework for solving both local and nonlocal effective transport equations. Particle tracking algorithms (PTAs) are used routinely to control numerical dispersion in solutions of the ADE (1) [25–29] and, more recently, to solve nonlocal effective transport equations based on CTRW [30–33], fADE [34], and multirate mass transfer [35,36]. Advantages and disadvantages of using PTAs to solve the ADE (1), e.g., the challenges posed by local mass conservation and a large number of particles that are needed to obtain smooth concentration profiles, are discussed in [37]. Solving nonlocal effective models with PTAs does not relax the assumptions that are required for their derivation.

We introduce a particle-based approach for modeling non-Fickian (anomalous) transport in heterogeneous environments that requires no assumptions about statistical properties of the model parameters. To increase the computational efficiency and accuracy of the particle-based simulations, we employ the convolution-based particle tracking (CBPT) method [38]. An added benefit of the proposed approach lies in its ability to convert any existing (legacy) particle tracking code into a simulator capable of handling non-Fickian behavior.

Particle tracking algorithms for solving the ADE (1) utilize its equivalence to the Langevin equation, which describes a solute particle's trajectory as a stochastic process [39]. Introducing a randomized time step into this process yields a new "subordinated" stochastic process that is capable of capturing anomalous transport behavior (e.g., [40]). This subordinated process is described by a set of Langevin equations, which represent a CTRW (e.g., [41]). In this paper, we adopt a general Langevin approach that imposes no statistical restrictions on the stochastic processes representing the spatial and temporal random increments. Each of these two processes can be correlated, non-stationary, and cross-correlated with the other, as well as have arbitrary distributions.

Employing this subordination strategy, we obtain a simple method to convert any random walk particle tracking simulator into a continuous time random walk simulator. This enables us to achieve two computational advantages. First, the proposed approach is non-intrusive in that it allows one to use any existing particle tracking simulator for modeling non-Fickian behavior. Second, the proposed approach is applicable to heterogeneous and non-stationary fields, whereas standard continuum formulations of non-Fickian transport require stationarity and statistical homogeneity. For stationary and uncorrelated random increments the well-known partial differential equation (PDE) formulations of CTRW in terms of generalized Fokker–Planck equations [23] can be obtained by a generalized Kramers–Moyal expansion. The two components of the proposed approach, CBPT and CTRW, are described in Sections 2 and 3, respectively. The computational algorithm is presented in Section 3.1. Section 4.1 contains a computational example that can be solved analytically and, hence, is used to analyze the accuracy and robustness of our algorithm. In Section 4.2, we apply the algorithm to model non-Fickian transport in two separate three-dimensional macroscopically heterogeneous porous media; the simulation results are contrasted with those obtained by solving the classical ADE (1). Section 5 provides a brief summary of the results and conclusions.

2. Convolution-based particle tracking (CBPT)

A standard random walk particle tracking (e.g., [28]) solves the ADE (1) by utilizing the equivalence between the ADE and the following Langevin equation (e.g., [39])

$$\mathbf{X}(t + \Delta t) = \mathbf{X}(t) + \mathbf{A}[\mathbf{X}(t)]\Delta t + \mathbf{B}[\mathbf{X}(t)] \cdot \boldsymbol{\xi}\sqrt{\Delta t}. \tag{2}$$

Here $\mathbf{X}(t) = [X_1(t), X_2(t), X_3(t)]^T$ is the random particle location at time t, $\boldsymbol{\xi} = [\xi_1, \xi_2, \xi_3]^T$ is Gaussian white noise with zero mean and unit variance,

$$\langle \xi_i \rangle = 0, \quad \langle \xi_i \xi_j \rangle = \delta_{ij}. \tag{3}$$

The drift vector $\mathbf{A}$ and the second-order tensor $\mathbf{B}$ are related to the coefficients in (1) by (e.g., [25])

$$\mathbf{A} = \mathbf{v} + \nabla \mathbf{D}, \quad \mathbf{B}\mathbf{B}^T = 2\mathbf{D}. \tag{4}$$

The particle's initial position, or its label, is given by $\mathbf{X}(t = 0) = \mathbf{x}_0$.

The CBPT [38] accelerates the convergence of the particle tracking algorithm (2)–(4), i.e., requires fewer particles, by taking advantage of the linearity of the ADE (1). Let $g(\mathbf{x}, t - \tau | \mathbf{x}_0)$ denote the Green's function for (1), which is defined as a solution of the adjoint equation

$$\frac{\partial g}{\partial \tau} = \nabla \cdot (\mathbf{D}\nabla g) + \mathbf{v} \cdot \nabla g, \tag{5}$$

subject to the initial condition $g(\mathbf{x}, \tau = t|\mathbf{x}_0) = \delta(\mathbf{x} - \mathbf{x}_0)$ and appropriate homogeneous boundary conditions. The Green's function $g(\mathbf{x}, t|\mathbf{x}_0)$ can be expressed in terms of particle trajectories as (e.g., [39])

$$g(\mathbf{x}, t|\mathbf{x}_0) = \langle \delta[\mathbf{x} - \mathbf{X}(t)]\rangle|_{\mathbf{X}(0)=\mathbf{x}_0}, \tag{6}$$

where the angular brackets denote the ensemble average over the random vector ξ. We use the particle tracking algorithm (2)–(4) to compute the Green's function $g(\mathbf{x}, t - \tau|\mathbf{x}_0)$ in (5) and (6).

Concentration $c(\mathbf{x}, t)$ resulting from spatially and/or temporally distributed sources $\dot{m}(\mathbf{x}', t')$ can now be computed as

$$c(\mathbf{x}, t) = \int_0^t \int_\Omega \dot{m}(\mathbf{x}_0, \tau)g(\mathbf{x}, t - \tau|\mathbf{x}_0)\mathrm{d}\mathbf{x}_0\mathrm{d}\tau, \tag{7}$$

where Ω is the computational domain. The accuracy and computational efficiency of the CBPT (2)–(7) are analyzed in detail in [38]. For the computational example described in Section 4.1, the performance of the CBPT algorithm is demonstrated in Table 1.

The performance metric ϵ in Table 1 is defined as

$$\epsilon = \frac{1}{N}\sqrt{\sum_{i=1}^{N}\left[\frac{c_{\mathrm{ex}}(\mathbf{x}_i) - c_{\mathrm{nu}}(\mathbf{x}_i)}{c_{\mathrm{ex}}(\mathbf{x}_i)}\right]^2}, \tag{8}$$

where c_{ex} is the "exact" concentration computed with an analytical solution, c_{nu} is the concentration predicted by a numerical method, i.e., by either the CBPT or the conventional particle tracking method, and N is the number of observations. It can be seen that the CBPT method is always at least as accurate as the conventional particle tracking methods and needs fewer particles to achieve the same accuracy in most cases, especially for larger solute injection times. The concentration as a function of distance from the center of the plume is plotted in Fig. 1.

3. Continuous time random walk (CTRW)

The random walk model (2)–(4) treats the time step $\tau \equiv \Delta t$ as deterministic and the transition length vector ξ as random, which results in Fickian dispersion. Let us introduce the randomized or operational time $s(t)$ (e.g., [40]) defined as a "renewal process" (e.g., [42,43]) that is conjugate to

$$\frac{\mathrm{d}t(s)}{\mathrm{d}s} = \tau(s), \tag{9}$$

Table 1
Performance metrics for the CBPT and conventional particle tracking methods.

Number of particles	Duration of mass injection (years)	CBPT method, ϵ	Conventional method, ϵ
10^5	1000	0.0154	0.433
10^5	100	0.0301	0.177
10^5	10	0.0698	0.0925
10^5	1	0.122	0.119
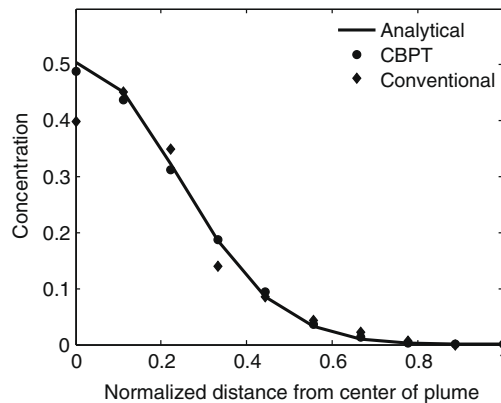
Fig. 1. Concentration $c(x_1, t)$ at time t = 1000 yr predicted with the analytical solution, the conventional particle tracking method, and the CBPT.

where $\tau(s)$ is a random process to be specified below. The random trajectory becomes an implicit function of time, $\mathbf{X}[s(t)]$. Thus, we obtain the subordinated system of Langevin equations (e.g., [41])

$$\mathbf{X}(s_n + \Delta s) = \mathbf{X}(s_n) + \mathbf{A}[\mathbf{X}(s_n)]\Delta s + \mathbf{B}[\mathbf{X}(s_n)] \cdot \xi(s_n)\sqrt{\Delta s}, \tag{10a}$$

$$t(s_n + \Delta s) = t(s_n) + \tau(s_n)\Delta s, \tag{10b}$$

where $\mathbf{A}$ and $\mathbf{B}$ are defined in (4), Δs is the constant increment of the discretized operational time $s_n = n\Delta s$.

In general, the random series $\{\xi(s_n)\}$ and $\{\tau(s_n)\}$ can be correlated or uncorrelated, stationary or non-stationary, and have arbitrary distributions.

As pointed out in the Introduction, this formulation is quite general and provides an alternative to PDE formulations of CTRW that assume statistical stationarity and independence of the stochastic processes $\xi(s)$ and $\tau(s)$. Furthermore, note that PDE formulations in terms of nonlocal Fokker–Planck equations typically rely on the truncation of a Kramers–Moyal expansion after the second-order term (e.g., [21,39]). The validity of this truncation in the CTRW framework for a Gaussian white noise $\xi(s)$ has been demonstrated in [30] by using random walk particle tracking simulations.

To facilitate the comparison with the existing CTRW literature, in the following we take each of the processes $\xi(s)$ and $\tau(s)$ to be uncorrelated and characterized by the joint probability density

$$\mathscr{P}\Big[\{\xi(s_n); \tau(s_n)\}_{n=1}^N\Big] = \prod_{n=1}^{N} \psi[\xi(s_n), \tau(s_n)], \tag{11}$$

where $\psi(\xi, \tau)$ is the joint transition length and time distribution density. The principal of causality requires that the temporal random process satisfy the condition $t(s_{n+1}) \geqslant t(s_n)$, which implies that $\tau(s_n) \geqslant 0$. The system of Langevin equations (10) describes particle motion as a CTRW in a macroscopically heterogeneous medium.

The choice of the probability density $\psi(\xi, \tau)$ is crucial to simulating non-Fickian transport in (randomly) heterogeneous environments, which are characterized by evolving hierarchies of length scales.

Some approaches and criteria for computing or selecting $\psi(\xi, \tau)$ can be found in [22,44]. Here we consider random walks that are mutually uncorrelated in space and time, so that the joint probability density $\psi(\xi, \tau)$ can be decoupled, i.e., $\psi(\xi, \tau) = \psi_s(\xi)\psi_t(\tau)$.

Furthermore, in the following we assume that transition times on a deterministic time interval $[t_1, t_2]$ follow a truncated power-law distribution (e.g., [30,45])

$$\psi_t(\tau) = \frac{r^\beta (1 + \tau/t_1)^{-1-\beta}}{t_1 \Gamma(-\beta, r)} e^{-r-\tau/t_2}, \quad r = \frac{t_1}{t_2}, \qquad 0 \leqslant \beta \leqslant 2, \tag{12}$$

where $\Gamma(a, x)$ is the incomplete Gamma function. The median transit time is set equal to the increment of the operational time, $t_1 = \Delta s$. For times $\tau > t_2, \psi_t(\tau)$ decreases exponentially fast. The transport behavior is anomalous in the transition regime $t_1 \leqslant t \leqslant t_2$ and becomes Fickian for large times $t > t_2$.

3.1. Simulation algorithm

The Green's function $\bar{g}(\mathbf{x}, t|\mathbf{x}_0)$ is given in terms of the particle trajectories of the CTRW (10) by

$$\bar{g}(\mathbf{x}, t|\mathbf{x}_0) = \langle \delta\{\mathbf{x} - \mathbf{X}[s(t)]\}\rangle|_{\mathbf{X}(0)=\mathbf{x}_0}, \tag{13}$$

where the angular brackets denote the average over the spatial and temporal random processes $\xi(s)$ and $\tau(s)$. Note that the particle trajectory here is an implicit function of time, $\mathbf{X}(t) \equiv \mathbf{X}[s(t)]$. Expression (13) can be written as

$$\bar{g}(\mathbf{x}, t|\mathbf{x}_0) = \int_0^\infty \langle \delta[\mathbf{x} - \mathbf{X}(s)]\delta[s - s(t)]\rangle|_{\mathbf{X}(0)=\mathbf{x}_0}\mathrm{d}s. \tag{14}$$

We discretize the operational time s according to $s_n = n\Delta s$ and $s(t) = N_t \Delta s$, where the discrete process N_t is defined by

$$N_t = \min(n|t(s_{n+1}) > t). \tag{15}$$

Thus, we obtain for $\bar{g}(\mathbf{x}, t|\mathbf{x}_0)$ the expression [46]

$$\bar{g}(\mathbf{x}, t|\mathbf{x}_0) = \sum_{n=0}^\infty \langle \delta[\mathbf{x} - \mathbf{X}(s_n)]\delta_{n,N_t}\rangle|_{\mathbf{X}(0)=\mathbf{x}_0} = \langle \delta[\mathbf{x} - \mathbf{X}(s_{N_t})]\rangle|_{\mathbf{X}(0)=\mathbf{x}_0}, \tag{16}$$

where $\langle \delta_{n,N_t}\rangle$ is the distribution of the renewal process N_t, i.e., the probability to make n steps up to time t.

This relation provides a straightforward recipe on how to obtain $\bar{g}(\mathbf{x}, t)$. The solution for the concentration profile for a general source distribution then is calculated by the convolution of the source term with $\bar{g}$ as expressed by (7). The corresponding algorithm combines the CBPT and CTRW approaches and consists of the following steps.

1. Starting from a point source at $\mathbf{x}_0$ at time $t = 0$, the spatio-temporal particle trajectories are tracked according to (10). After N_t steps, that is, when the simulation time t is between t_N and t_{N+1}, $t_N \leqslant t < t_{N+1}$, the position $\mathbf{x}_N$ is recorded. The Green's function $\bar{g}$ is determined by sampling the particle positions in space according to (16).
2. Finally, the anomalous concentration profile is obtained by convolving $\bar{g}$ with the source term.

This algorithm renders itself to straightforward integration into most existing legacy codes, as we do below for the DOE-certified code Finite Element Heat and Mass Transfer Code (FEHM) [47]. Next, we apply this code to three computational examples of increasing difficulty. The example in Section 4.1 is used to demonstrate the accuracy and computational efficiency of the CBPT. Section 4.2 provides two examples of the use of the CBPT-CTRW to model anomalous transport in realistic three-dimensional geological settings.

3.2. Integration into legacy codes

FEHM is a multiphase, multidimensional reservoir simulator. In order to calculate the velocity field, FEHM simulations may include numerous coupled processes including thermo-hydro-chemical-mechanical (THCM). These coupled processes are often important for studies of carbon sequestration, nuclear waste disposal, and hazardous waste disposal. FEHM currently lacks the capability of handling anomalous transport. It relies on a three-dimensional node-based particle tracking method that takes advantage of the fluxes at nodes being given by the flow solution, and can be used easily with unstructured grids, without having to use interpolation schemes. The particle tracking algorithm takes advantage of the complex velocity field calculated by the flow simulation that often depends on the numerous coupled processes mentioned above. The proposed algorithm can be used with any node based particle tracking technique.

4. Transport in macroscopically homogeneous and heterogeneous media

In this section, we apply the random walk algorithm presented above to transport in macroscopically homogeneous and heterogeneous media. The code is validated against known solutions for instantaneous sources in macroscopically homogeneous media [30] and applied to solute transport evolving from continuous solute injections in macroscopically homogeneous and heterogeneous media.

4.1. Macroscopically homogeneous medium

Consider solute transport in a three-dimensional macroscopically homogeneous porous medium $\Omega = [0, \infty] \times [0, L_2] \times [0, L_3]$. Flow velocity $\mathbf{v}$ is taken to be constant and aligned with the x_1 coordinate axis, $\mathbf{v} = [v, 0, 0]^T$ with $v = 34.2$ m/yr. The longitudinal dispersivity is set to $\alpha_L = 500$ m, the corresponding longitudinal dispersion coefficient is $D_L = \alpha_L v$, and the transverse horizontal and vertical dispersion are neglected, $D_T = 0$. Constant head boundaries are prescribed at the inlet and outlet, with a difference in head of 0.377 MPa. The porosity and permeability are constant throughout the medium with values of $\omega = 0.03361$ and $k = 10^{-12}$ m^2, respectively. The parameters are chosen such that the resulting flow translates into a mean travel time of 500 yr to reach the outlet. Regardless of the transport model used, this parameter choice renders transport one-dimensional, $c(\mathbf{x}, t) = c(x_1, t)$.

The initial concentration is set to $c(x_1, t = 0) = 0$. The boundary condition at $x_1 = 0$ is more conveniently expressed in terms of the flux-averaged concentration [48]

$$c_f(x_1, t) = v^{-1} \int_0^{x_1} \frac{\partial c(x_1', t)}{\partial t} \, dx_1'. \tag{17}$$

At the inlet $x_1 = 0$, $c_f(x_1, t)$ is given by

$$c_f(x_1 = 0, t) = j(t)/v, \tag{18}$$

where $j(t)$ is the boundary flux. The concentration and concentration flux are zero at the boundary at infinity. We study transport in terms of spatial profiles, that is snapshots of $c(x_1, t)$ and breakthrough curves at a given distance. The latter are equivalent to first passage time distributions at a control plane. They are obtained from the flux-averaged concentration. In these simulations, the domain Ω is discretized with grid spacings $\Delta x_1 = 400$ m.

4.1.1. Validation of the simulation algorithm

Here, we validate the simulation algorithm against known solutions for the flux-averaged concentration $c_f(x_1, t)$ with a constant, continuous injection at the inlet, that is, $j(t) = v$ at $x_1 = 0$ using a total of 10^4 particles. For stationary and uncorrelated random increments, the CTRW (10) admits a PDE representation in terms of a temporally nonlocal Fokker–Planck equation (e.g., [21,23,30]). Dentz et al. [30] studied resident and flux-averaged concentrations for anomalous transport in a macroscopically homogeneous medium using random walk simulations as well as Laplace space solutions of the equivalent generalized Fokker–Planck equations. For the above specified boundary and initial conditions, the Laplace transform of the flux-averaged concentration is given by

$$\tilde{c}_f(x_1, \lambda) = \exp\left[-\frac{v x_1}{2 D_L}\left(\sqrt{1 + 4\frac{\lambda D_L}{\widetilde{M} v^2}} - 1\right)\right]. \tag{19a}$$

Here the tilde indicates Laplace transforms, λ is the Laplace variable, $\widetilde{M}$ is the Laplace transform of the memory function defined as

$$\widetilde{M}(\lambda) = \frac{t_1 \lambda \tilde{\psi}_t(\lambda)}{1 - \tilde{\psi}_t(\lambda)}, \tag{19b}$$

and $\tilde{\psi}_t(\lambda)$ is the Laplace transform of $\psi_t(t)$ in (12). The Laplace transform of the concentration $c(x_1, t)$ given by a solution of the ADE (1) is recovered from (19a) by setting $\widetilde{M} \equiv 1$.

The analytical solution (19) is used to analyze the convergence of the CBPT and to validate the particle tracking implementation of the CTRW (10)–(12) (the simulation algorithm in Section 3.1). Fig. 2 compares the accuracy of the CBPT for both classical (Fig 2a) and anomalous (Fig 2b) transport. In the latter case, the CBPT is an integral part of the CBPT-CTRW algorithm described in Section 3.1. In both cases, the Laplace transform (19) of concentration for the analytical solution is inverted with the algorithm of de Hoog et al. [49].

The breakthrough is computed at a distance of $x = 15.2$ km over a total time of 3000 yr. The results from both analytical and numerical (the CBPT-CTRW algorithm) simulations are plotted in Fig. 2 for the ADE and $\beta = 1.25$. The analytical solutions shown as circles and the numerical solutions represented by solid lines are in excellent agreement with each other. Such continuous injection scenarios are of practical importance for the modeling of contamination events in industrial plants, where contaminants can leak into the subsurface over many years, underground nuclear waste storage, as well as for the modeling of heat plumes in the subsurface that are generated by heat exchangers.

4.1.2. Breakthrough curves and spatial profiles

An often neglected aspect of contaminant transport is the spatial nature of the plume across the entire field of study, because PTAs are concerned mostly with the breakthrough across a control plane. In this section, we present both breakthrough curves as well as the spatial concentration distribution for pulse injection $j(t) = v\delta(t)$ at the inlet $x_1 = 0$.

As in [30], we study the effects on anomalous transport of the three key parameters in the CTRW model defined by the truncated power-law waiting time distribution (12): the median waiting time t_1, the cut-off time t_2 after which transport becomes Fickian, and the exponent β.

Consequently, we set $t_1 = 4$ yr and $t_2 = 10^4$ yr, and focus on the effects of $0 \leqslant \beta \leqslant 2$. It has been shown (e.g., [22]) that $\beta = 2$ asymptotically leads to the Fickian behavior as predicted with the ADE (1) and that deviations from the Fickian transport become stronger as β becomes smaller.

Fig. 3 depicts the breakthrough curves resulting from the pulsed boundary condition, $c(0, t) \equiv 1$ for $t \leqslant 10^3$ yr and $c(0, t) \equiv 0$ for $t > 10^3$ yr. The breakthroughs computed with the particle tracking simulations of the classical and anomalous transport are shown for several values of β.

In accordance with the theory, $\beta = 2$ gives rise to the classical transport behavior in terms of breakthrough times, peak concentrations, and Gaussianity of concentration profiles. As β decreases, breakthrough times become larger and concentration profiles exhibit progressively longer tails. The peak breakthrough values of concentration become progressively smaller, since the area under the breakthrough curves (i.e., total mass) is constant. The number of particles that is required to represent breakthrough curves within a given tolerance level increases as β decreases and the deviation from the Gaussian behavior becomes more pronounced.
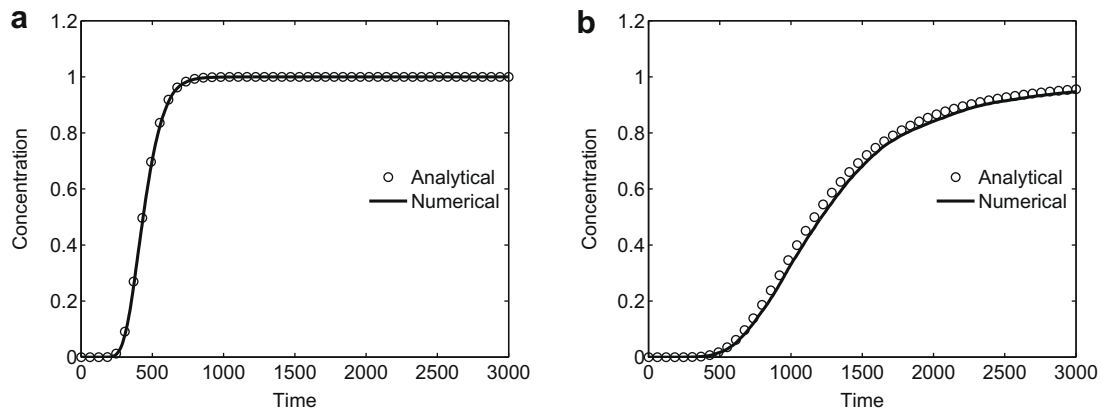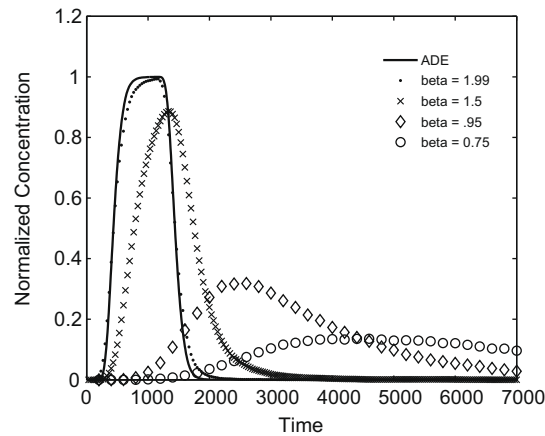

Fig. 2. The breakthrough curves at $x_1 = 15.2$ km predicted with (a) the classical and (b) anomalous ($\beta = 1.25$) models of transport.

Fig. 3. Breakthrough curves of concentration $c(x_1, t)$ at $x_1 = 15.2$ km for the pulsed input at the inlet $x_1 = 0$.

Fig. 4 exhibits the temporal evolution of the concentration profiles for several values of β. The classical transport model (ADE or $\beta = 2$) exhibits no tailing and predicts that the solute occupies the entire computational domain by $t = 2000$ yr. For $\beta = 1.99$, the tailing is very small and most of the mass has broken through by $t = 2000$ yr and all of it by $t = 3000$ yr. While $\beta = 1.5$ leads to a significant tailing, the arrival at the outlet starts to taper off by 2000 yr. The concentration profiles corresponding to $\beta < 1$ indicate that mass is still breaking through at the end of the simulation time.

Fig. 4 also reveals that the concentration at the inlet $x_1 = 0$ increases with decreasing β. This is because smaller values of β correspond to larger residence times in a boundary cell, resulting in a slower rate of transport across the medium and hence later arrival at the cross-section $x_1 = 15.2$ km. This is a mathematical representation of subscale mass transfer processes, such as diffusion into dead-end pores, which retard the solute migration.
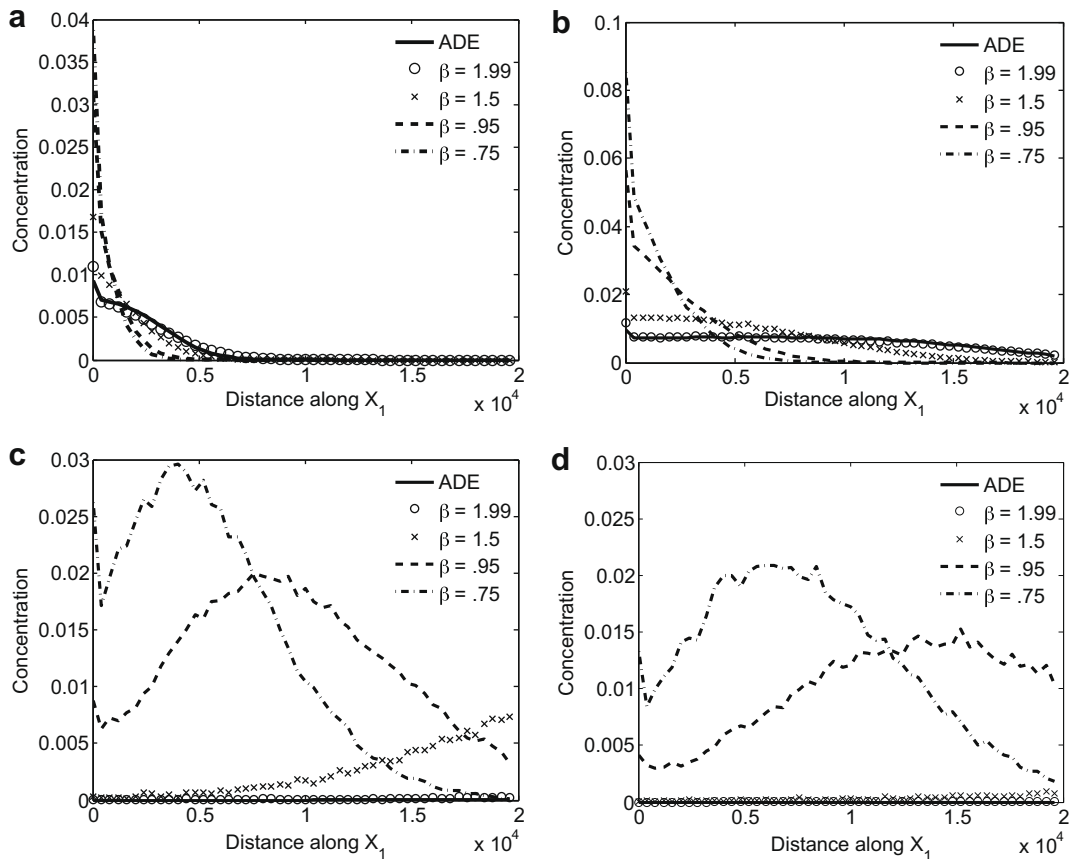
Fig. 4. Concentration profiles $c(x, t)$ at (a) $t = 100$ yr, (b) $t = 500$ yr, (c) $t = 2000$ yr, and (d) $t = 3000$ yr for pulsed input at the inlet.

4.2. Macroscopically heterogeneous medium

We use the CBPT-CTRW algorithm to simulate anomalous transport in heterogeneous media using two examples presented here. We consider in both examples a three-dimensional heterogeneous porous medium $\Omega = [0,L_1] \times [0,L_2] \times [0,L_3]$. The simulation results presented below correspond to $L_1 = 20$ km, $L_2 = 9.6$ km and $L_3 = 5$ km.

In the first example, the model was divided into 4 equal zones in the primary flow direction, spanning 5 km each. The first and fourth zones have the same properties as the homogeneous medium example of the previous section. The second zone has a reduced porosity of $\omega = 0.01425$ and the third zone a reduced permeability of $k = 10^{-13}$ m^2. The simulations below correspond to $H_1 - H_2 = 0.377$ MPa. The other boundaries are impermeable to flow. To solve the flow equation (20) with the finite element code FEHM, the domain is discretized with a total of $51 \times 25 \times 101 = 128,775$ nodes in the x_1, x_2, and x_3 directions, respectively. The transport equations were solved using 10^4 particles.

Lower porosities result in faster movement of particles through zone 2. The overall flow is slower, as a result of the lower permeability across one of the four zones, since the effective permeability is a harmonic mean of the different permeability values. The breakthrough point for these simulations was at $L_1 = 15.2$ km. The simulation was performed for 3000 yr and tracer was injected continuously for the entire period of the simulation. The breakthrough curve (Fig. 5) is shown for the ADE as well as for the case of $\beta = 1.25$.

This example demonstrates the effects of large scale heterogeneity on contaminant transport. Features such as high permeability faults or low permeability clay lenses can be represented in this manner.

In the second example, we take a geostatistical approach for representing heterogeneity. In the subsurface, permeability fields $k(\mathbf{x})$ often follow a log-normal distribution and are correlated. The mean, variance, and correlation length are quantities that can be obtained from field measurements. These parameters can then be used to generate synthetic permeability fields. In the second case studied, in addition to the longitudinal dispersion coefficient specified in Section 4.1, we define the transverse dispersion coefficient as $D_T = \alpha_T |\mathbf{v}|$ where the transverse dispersivity is set to $\alpha_T = 50$ m. We specify a pulse boundary condition at the inlet, injecting 10^4 particles uniformly over a 100 m distance at the top edge, $x_1 = 0$, $x_2 = L_2$.

The medium's permeability $k(\mathbf{x})$ – the top subfigure in Fig. 6 – was constructed using a multiresolution random field generator based on the Karhunen–Loéve decomposition [50]. It represents a realization of the statistically homogeneous random field that has the mean $\bar{k} = 10^{-12}$ m^2, transformed variance $\sigma_{\ln k}^2 = 1$, and anisotropic exponential covariance function with correlation lengths 200 m, 200 m, and 100 m in the x_1, x_2 and x_3 directions, respectively. Tracer was injected for the first 1000 yr of the simulation.

The heterogeneity of the medium causes spatial variability of the fluid velocity $\mathbf{v}(\mathbf{x})$. It is computed by rescaling the Darcy flux $\mathbf{q}(\mathbf{x})$ with the medium's (constant) porosity ω, i.e., $\mathbf{v} = \mathbf{q}/\omega$. The Darcy flux is given by a solution of the steady-state flow equation,

$$\mathbf{q} = -\frac{kg}{v}\nabla h, \quad \nabla \cdot \mathbf{q} = 0, \tag{20}$$

where v is the fluid's kinematic viscosity, g is the gravitational constant and $h(\mathbf{x})$ is the hydraulic head. The flow is driven by the hydraulic head gradient resulting from boundary conditions $h(x_1 = 0, x_2, x_3) = H_1$ and $h(x_1 = L_1, x_2, x_3) = H_2$. The other boundary conditions and domain discretization for this example were identical to those used in the previous heterogeneous medium example.

The results of these simulations are presented in Fig. 6 for anomalous transport with $\beta = 1.5$ and $\beta = 0.95$, as well as for the ADE model of transport. Iso-surface plots of the model domain are shown at various times, 100 yr, 600 yr and 1200 yr. A normalized concentration of 0.0025 was chosen for the isoline with the ADE plume shown in red and the CBPT-CTRW shown
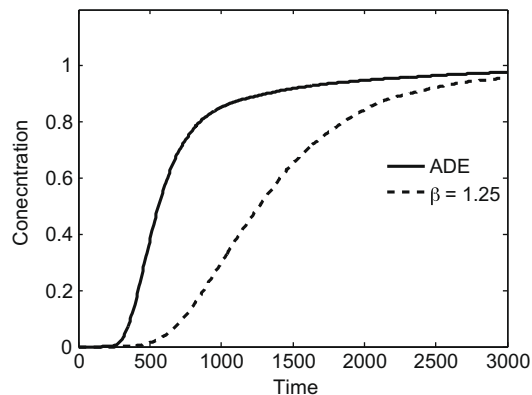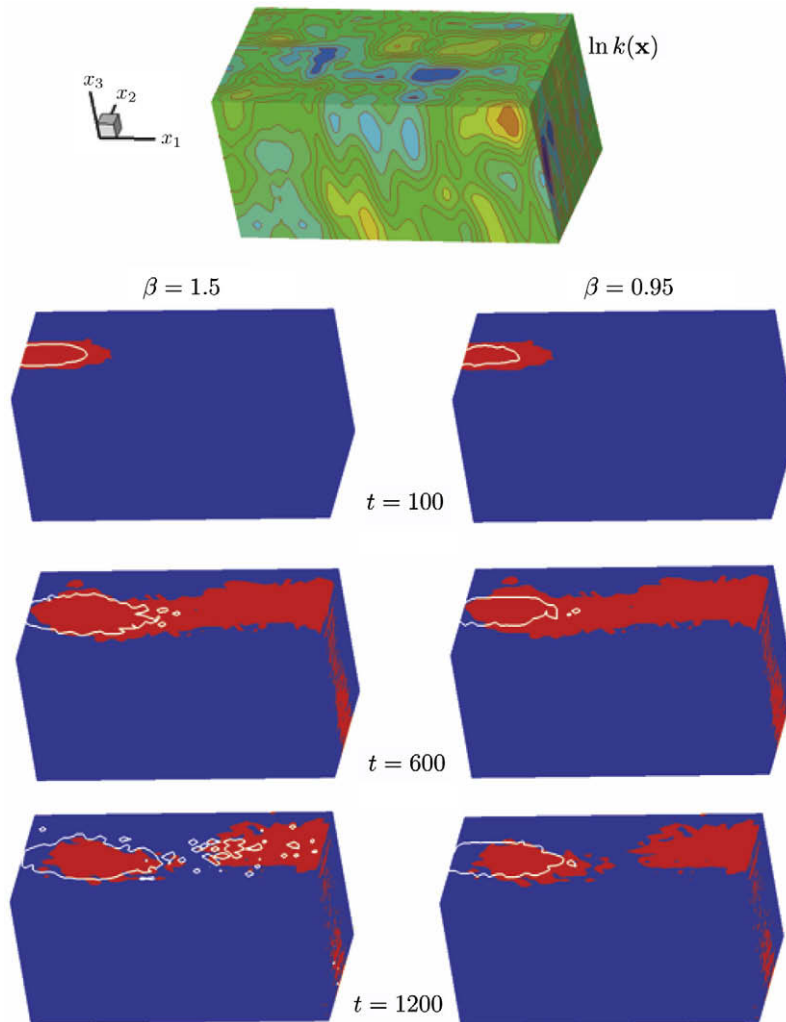

Fig. 5. Comparison of the ADE and CTRW methods for flow through heterogeneous medium. Breakthrough curves of concentration $c(x_1, t)$ at $x_1 = 15.2$ km for continuous injection at the inlet $x_1 = 0$.

Fig. 6. Comparison of the ADE and CTRW methods for flow through heterogeneous permeability field. The ADE plume is shown in red and the CTRW plume in white. (For interpretation of the references to colour in this figure legend, the reader is referred to the web version of this article.)

in white. Because the tracer is injected near the top surface of the domain, the majority of the plumes travel along the top surface of the model domain. As time progresses, the plume appears to break apart into "islands" at the top surface. The islands are due to the fact that low permeability zones cause the plume to leave the top surface and to reappear later due to high permeability pathways. The CBPT-CTRW algorithm predicts significant attenuation of the plume for both values of β. It resulted in lower peak concentration and longer tail breakthrough curves than those resulting from the ADE. Lower values of β lead to higher values of the inlet concentration at later times, since they correspond to larger residence times in a cell. The distance traveled by the plume also decreases as β decreases. Relative to its counterpart predicted with the ADE, it spreads farther in the transverse direction.

5. Conclusions

Advection–dispersion equations (ADEs) are routinely used to describe transport phenomena in heterogeneous environments. Yet they often fail to capture subgrid heterogeneities that lead to the so-called anomalous or non-Fickian transport behavior, whose manifestations are early or late arrival times, long tails of concentration profiles, etc.

We presented a particle-based approach for modeling non-Fickian (anomalous) transport in heterogeneous environments. The approach treats a particle trajectory as a subordinated stochastic process that is described by a set of Langevin equations, which represent a CTRW at its basic level. To increase the computational efficiency and accuracy of these simulations, we employ the convolution-based particle tracking (CBPT) method.

Our analysis leads to the following major conclusions.

1. The Langevin formulation used in the CTRW–CBPT algorithm is general in that no statistical restrictions are imposed on the stochastic processes representing the spatial and temporal random increments. They can be correlated in space and time, stationary or non-stationary, their distributions are arbitrary.
2. For stationary and uncorrelated random increments, the well-known partial differential equation (PDE) formulations of CTRW in terms of generalized Fokker–Planck equations can be obtained by a generalized Kramers–Moyal expansion.
3. The CTRW–CBPT algorithm reproduces analytical solutions for both classical (ADE-based) and anomalous (a PDE formulation of CTRW) transport models, with CBPT providing a significant computational speed-up.
4. Finally, the CTRW–CBPT approach enables one to convert any existing particle tracking code into a simulator capable of handling non-Fickian (anomalous) transport in large field-scale problems that exhibit complex parameter structures (e.g., realistic geological settings) and complex flow fields.

Acknowledgments

References

[1] J. Bear, Dynamics of Fluids in Porous Media, Elsevier, New York, 1972.
[2] D. Stein, F.H.J. vander Heyden, W.J.A. Koopmans, C. Dekker, Pressure-driven transport of confined DNA polymers in fluidic channels, Proc. Natl. Acad. Sci. 103 (43) (2006) 15853–15858.
[3] S. Koennings, J. Tessmar, T. Blunk, A. Göpferich, Confocal microscopy for the elucidation of mass transport mechanisms involved in protein release from lipid-based matrices, Pharm. Res. 24 (7) (2007) 1325–1335, doi:10.1007/s11095-007-9258-8.
[4] F.J. Rueda, S.G. Schladow, J.F. Clark, Mechanisms of contaminant transport in a multi-basin lake, Ecol. Appl. 18 (8) (2008) A72–A88.
[5] L.W. Gelhar, Perspectives on field-scale application of stochastic subsurface hydrology, in: G. Dagan, S.P. Neuman (Eds.), Subsurface Flow and Transport: A Stochastic Approach, Cambridge University Press, New York, 1997, pp. 157–176.
[6] S.P. Neuman, Adaptive Eulerian–Lagrangian finite element method for advection–dispersion, Int. J. Numer. Methods Eng. 20 (2) (1984) 321–337.
[7] A. Younes, M. Fahs, P. Ackerer, A new approach to avoid excessive numerical diffusion in Eulerian–Lagrangian methods, Commun. Numer. Methods Eng. 24 (11) (2008) 897–910.
[8] E.R. Ewing, H. Wang, A summary of numerical methods for time-dependent advection-dominated partial differential equations, J. Comput. Appl. Math. 128 (1–2) (2001) 423–445.
[9] G. Seisenberger, M.U. Ried, T. Endress, H. Buning, M. Hallek, C. Brauchle, Real-time single-molecule imaging of the infection pathway of an adeno-associated virus, Science 94 (5548) (2001) 1929–1932.
[10] A. Cortis, B. Berkowitz, Anomalous transport in "classical" soil and sand columns, Soil Sci. Soc. Am. J. 68 (5) (2004) 1539–1548.
[11] I.M. Tolic-Norrelykke, E.-L. Munteanu, G. Thon, L. Oddershede, K. Berg-Sorensen, Anomalous diffusion in living yeast cells, Phys. Rev. Lett. 93 (7) (2004) 078102-1–078102-4.
[12] Y. Zhang, D.A. Benson, Lagrangian simulation of multidimensional anomalous transport at the MADE site, Geophys. Res. Lett. 35 (2008) L07403, doi:10.1029/2008GL033222.
[13] B. Berkowitz, H. Scher, Theory of anomalous chemical transport in fracture networks, Phys. Rev. E 57 (5) (1998) 5858–5869.
[14] J.H. Cushman, M. Moroni, Statistical mechanics with three-dimensional particle tracking velocimetry in the study of anomalous dispersion. I. Theory, Phys. Fluids 13 (1) (2001) 75–80.
[15] P. Salamon, D. Fernàndez-Garcia, J.J. Gómez-Hernández, Modeling tracer transport at the MADE site: the importance of heterogeneity, Water Resour. Res. 43 (2007) W08404.
[16] E. Morales-Casique, S.P. Neuman, A. Guadagnini, Nonlocal and localized analyses of nonreactive solute transport in bounded randomly heterogeneous porous media: theoretical framework, Adv. Water Resour. 29 (8) (2006) 1238–1255.
[17] M. Dentz, D.M. Tartakovsky, Self-consistent four-point closure for transport in steady random flows, Phys. Rev. E 77 (6) (2008), doi:10.1103/PhysRevE.77.066307.
[18] M.M. Meerschaert, D.A. Benson, B. Baumer, Multidimensional advection and fractional dispersion, Phys. Rev. E 59 (5) (1999) 5026–5028.
[19] M.M. Meerschaert, D.A. Benson, H.P. Scheffler, P. Becker-Kern, Governing equations and solutions of anomalous random walk limits, Phys. Rev. E 66 (2001) 060102(R).
[20] J. Klafter, R. Silbey, Derivation of continuous-time random-walk equations, Phys. Rev. Lett. 44 (2) (1980) 558.
[21] M. Dentz, B. Berkowitz, Transport behavior of a passive solute in continuous time random walks and multirate mass transfer, Water Resour. Res. 39 (5) (2003) 1111, doi:10.1029/2001WR001163.
[22] B. Berkowitz, A. Cortis, M. Dentz, H. Scher, Modeling non-Fickian transport in geological formations as a continuous time random walk, Rev. Geophys. 44 (2) (2006) RG2003.
[23] B. Berkowitz, J. Klafter, R. Metzler, H. Scher, Physical pictures of transport in heterogeneous media: advection–dispersion, random walk and fractional derivative formulations, Water Resour. Res. 38 (10) (2002) 1191, doi:10.1029/2001WR001030.
[24] A. Cortis, C. Gallo, H. Scher, B. Berkowitz, Numerical simulation of non-Fickian transport in geological formations with multiple–scale heterogeneities, Water Resour. Res. 40 (2004) W04209.
[25] W. Kinzelbach, The random walk method in pollutant transport simulation, in: E. Custodio, A. Gurgui, J.P. Lobo-Ferreira (Eds.), Groundwater Flow and Quality Modelling, D. Reidel Publ. Co., Norwell, Massachusetts, 1988, pp. 227–245.
[26] P.C. Lichtner, S. Kelkar, B.A. Robinson, New form of dispersion tensor for flow in axisymmetric media with implementation in particle tracking, Water Resour. Res. 38 (8) (2002) 21-1–21-16.
[27] M. Dentz, H. Kinzelbach, S. Attinger, W. Kinzelbach, Numerical studies of the transport behavior of a passive solute in a two-dimensional incompressible random flow field, Phys. Rev. E 67 (2003) 046306.
[28] F. Delay, P. Ackerer, C. Danquigny, Simulating solute transport in porous or fractured formations using random walk particle tracking: a review, Vadose Zone J. 4 (2005) 360–379.

[29] A. Younes, P. Ackerer, Solving the advection-diffusion equation with the Eulerian–Lagrangian localized adjoint method on unstructured meshes and non uniform time stepping, J. Comput. Phys. 208 (1) (2005) 384–402.
[30] M. Dentz, A. Cortis, H. Scher, B. Berkowitz, Time behavior of solute transport in heterogeneous media: transition from anomalous to normal transport, Adv. Water Resour. 27 (2004) 155–173.
[31] T. LeBorgne, P. Gouze, Non-Fickian dispersion in porous media: 2. Model validation from measurements at different scales, Water Resour. Res. 44 (2008) W06427.
[32] M. Dentz, H. Scher, D. Holder, B. Berkowitz, Transport behavior of coupled continuous-time random walks, Phys. Rev. E 78 (2008) 041110.
[33] Y. Edery, H. Scher, B. Berkowitz, Modeling bimolecular reactions and transport in porous media, Geophys. Res. Lett. 36 (2009) L02407, doi:10.1029/2008GL036381.
[34] Y. Zhang, D.A. Benson, M.M. Meerschaert, H.-P. Scheffler, On using random walks to solve the space-fractional advection–dispersion equations, J. Stat. Phys. 123 (1) (2006) 89–110.
[35] P. Salamon, D. Fernàndez-Garcia, J.J. Gómez-Hernández, Modeling mass transfer processes using random walk particle tracking, Water Resour. Res. 42 (2006) W11417.
[36] D.A. Benson, M.M. Meerschaert, A simple and efficient random walk solution of multi-rate mobile/immobile mass transport equations, Adv. Water Resour. 32 (2009) 532–539.
[37] P. Salamon, D. Fernàndez-Garcia, J.J. Gómez-Hernández, A review and numerical assessment of the random walk particle tracking method, J. Contam. Hydrol. 87 (3–4) (2006) 277–305.
[38] B.A. Robinson, Z.V. Dash, G. Srinivasan, A particle tracking transport method for the simulation of resident and flux-averaged concentration of solute plumes in groundwater models, Comput. Geosci., submitted for publication.
[39] H. Risken, The Fokker–Planck equation: methods of solution and applications, Springer Series in Synergetics, second ed., vol. 18, Springer, Berlin, Heidelberg, New York, 1996.
[40] M. Ting Lee, G.A. Whitmore, Stochastic processes directed by randomized time, J. Appl. Prob. 30 (1993) 302–314.
[41] H.C. Fogedby, Langevin eqations for continuous time Lévy flights, Phys. Rev. E 50 (1994) 1657–1660.
[42] W. Feller, A Introduction to Probability Theory and Its Applications, vol. II, John Wiley and Sons, 1971.
[43] C. Godrèche, J.M. Luck, Statistics of occupation time renewal processes, J. Stat. Phys. 104 (2001) 489–524.
[44] H. Scher, M. Lax, Stochastic transport in a disordered solid. I. Theory, Phys. Rev. B 7 (1973) 4491–4502.
[45] B. Berkowitz, H. Scher, Exploring the nature of non-Fickian transport in laboratory experiments, Adv. Water Resour. 32 (2009) 750–755.
[46] I.M. Sokolov, A. Blumen, J. Klafter, Dynamics of annealed systems under external fields: CTRW and the fractional Fokker–Planck equations, Europhys. Lett. 56 (2001) 175–180.
[47] H.S. Viswanathan, B.A. Robinson, A.J. Valocchi, I.R. Triay, A reactive transport model of neptunium migration from the potential repository at yucca mountain, J. Hydrol. 209 (1) (1998) 251–280.
[48] A. Kreft, A. Zuber, On the physical meaning of the dispersion equation and its solutions for different initial and boundary conditions, Chem. Eng. Sci. 33 (1978) 1471–1480.
[49] F.R. de Hoog, J.H. Knight, A.N. Stokes, An improved method for numerical inversion of Laplace transforms, SIAM J. Sci. Stat. Comput. 3 (1982) 357–366.
[50] C. Schwab, R.A. Todor, Karhunen–Loève approximation of random fields by generalized fast multipole methods, J. Comput. Phys. 217 (1) (2006) 100–122.